Flavor Decomposition of the Polarized Quark Distributions in the Nucleon from Inclusive and Semi-inclusive Deep-inelastic Scattering

The HERMES Collaboration

K. Ackerstaff[6], A. Airapetian[36], N. Akopov[36], I. Akushevich[7], M. Amarian[26,31,36], E.C. Aschenauer[7,14,26], H. Avakian[11], R. Avakian[36], A. Avetissian[36], B. Bains[16], S. Barrow[28], C. Baumgarten[24], M. Beckmann[13], S. Belostotski[29], J.E. Belz[32,33], Th. Benisch[9], S. Bernreuther[9], N. Bianchi[11], S. Blanchard[25], J. Blouw[26], H. Böttcher[7], A. Borissov[6,15], J. Brack[5], B. Bray[4], S. Brauksiepe[13], B. Braun[9,24], St. Brons[7], W. Brückner[15], A. Brüll[15], E.E.W. Bruins[21], H.J. Bulten[19,26,35], R.V. Cadman[16], G.P. Capitani[11], P. Carter[4], P. Chumney[25], E. Cisbani[31], G.R. Court[18], P. F. Dalpiaz[10], R. De Leo[3], P.P.J. Delheij[33], E. De Sanctis[11], D. De Schepper[2,21], E. Devitsin[23], P.K.A. de Witt Huberts[26], P. Di Nezza[11], M. Düren[9], A. Dvoredsky[4], J. Ely[5], G. Elbakian[36], J. Emerson[32,33], A. Fantoni[11], A. Fechtchenko[8], M. Ferstl[9], D. Fick[20], K. Fiedler[9], B.W. Filippone[4], H. Fischer[13], H.T. Fortune[28], B. Fox[5], S. Frabetti[10], J. Franz[13], S. Frullani[31], M.-A. Funk[6], N.D. Gagunashvili[8], P. Galumian[1], H. Gao[2,16,21], Y. Gärber[7], F. Garibaldi[31], G. Gavrilov[29], P. Geiger[15], V. Gharibyan[36], A. Golendukhin[6,20,24,36], G. Graw[24], O. Grebeniouk[29], P.W. Green[1,33], L.G. Greeniaus[1,33], C. Grosshauser[9], M. Guidal[26], A. Gute[9], V. Gyurjyan[11], J.P. Haas[25], W. Haeberli[19], J.-O. Hansen[2], D. Hasch[7], O. Häusser[†32,33], R. Henderson[33], F.H. Heinsius[13], Th. Henkes[26], M. Henoch[9], R. Hertenberger[24], Y. Holler[6], R.J. Holt[16], W. Hoprich[15], H. Ihssen[6,26], M. Iodice[31], A. Izotov[29], H.E. Jackson[2], A. Jgoun[29], C. Jones[2], R. Kaiser[7,32,33], M. Kestel[13], E. Kinney[5], M. Kirsch[9], A. Kisselev[29], P. Kitching[1], H. Kobayashi[34], N. Koch[20], K. Königsmann[13], M. Kolstein[26], H. Kolster[24], V. Korotkov[7], W. Korsch[4,17], V. Kozlov[23], L.H. Kramer[12,21], B. Krause[7], V.G. Krivokhijine[8], M. Kückes[33], F. Kümmell[13], M. Kurisuno[34], G. Kyle[25], W. Lachnit[9], W. Lorenzon[22,28], A. Lung[4], N.C.R. Makins[2,16], F.K. Martens[1], J.W. Martin[21], H. Marukyan[36], F. Masoli[10], A. Mateos[21], M. Maul[30], M. McAndrew[18], K. McIlhany[4,21], R.D. McKeown[4], F. Meissner[7], F. Menden[13,33], D. Mercer[5], A. Metz[24], N. Meyners[6], O. Mikloukho[29], C.A. Miller[1,33], M.A. Miller[16], R. Milner[21], V. Mitsyn[8], A. Most[16,22,28], R. Mozzetti[11], V. Muccifora[11], A. Nagaitsev[8], E. Nappi[3], Yu. Naryshkin[29], A.M. Nathan[16], F. Neunreither[9], J.M. Niczyporuk[16,21], W.-D. Nowak[7], M. Nupieri[11], P. Oelwein[15], H. Ogami[34], T.G. O'Neill[2], R. Openshaw[33], B.R. Owen[16], J. Ouyang[33], V. Papavassiliou[25], S.F. Pate[21,25], M. Pitt[4], H.R. Poolman[26], S. Potashov[23], D.H. Potterveld[2], G. Rakness[5], A. Reali[10], R. Redwine[21], A.R. Reolon[11], R. Ristinen[5], K. Rith[9], G. Röper[6], P. Rossi[11], S. Rudnitsky[22,28], M. Ruh[13], D. Ryckbosch[14], Y. Sakemi[34], I. Savin[8], C. Scarlett[22], A. Schäfer[30], F. Schmidt[9], H. Schmitt[13], G. Schnell[25], K.P. Schüler[6], A. Schwind[7], J. Seibert[13], T.-A. Shibata[34], K. Shibatani[34], T. Shin[21], V. Shutov[8], C. Simani[10], A. Simon[13,25], K. Sinram[6], P. Slavich[10,11], W.R. Smythe[5], J. Sowinski[15], M. Spengos[6,28], E. Steffens[9], J. Stenger[9], J. Stewart[18], F. Stock[9,15], U. Stoesslein[7], M. Sutter[21], H. Tallini[18], S. Taroian[36], A. Terkulov[23], D.M. Thiessen[32,33], B. Tipton[21], E. Thomas[11], A. Trudel[33], M. Tytgat[14], G.M. Urciuoli[31], J.J. van Hunen[26], R. van de Vyver[14], J.F.J. van den Brand[26,35], G. van der Steenhoven[26], M.C. Vetterli[32,33], V. Vikhrov[29], M. Vincter[33], J. Visser[26], E. Volk[15], W. Wander[9,21], T.P. Welch[27], J. Wendland[32,33], S.E. Williamson[16], T. Wise[19], K. Woller[6], S. Yoneyama[34], K. Zapfe[6], H. Zohrabian[36], R. Zurmühle[28]

[1] *Department of Physics, University of Alberta, Edmonton, Alberta T6G 2J1, Canada*
[2] *Physics Division, Argonne National Laboratory, Argonne, Illinois 60439-4843, USA*
[3] *Istituto Nazionale di Fisica Nucleare, Sezione di Bari, 70124 Bari, Italy*
[4] *W.K. Kellogg Radiation Lab, California Institute of Technology, Pasadena, California 91125, USA*
[5] *Nuclear Physics Laboratory, University of Colorado, Boulder, Colorado 80309-0446, USA*
[6] *DESY, Deutsches Elektronen Synchrotron, 22603 Hamburg, Germany*
[7] *DESY Zeuthen, 15738 Zeuthen, Germany*
[8] *Joint Institute for Nuclear Research, 141980 Dubna, Russia*
[9] *Physikalisches Institut, Universität Erlangen-Nürnberg, 91058 Erlangen, Germany*
[10] *Istituto Nazionale di Fisica Nucleare, Sezione di Ferrara and Dipartimento di Fisica, Università di Ferrara, 44100 Ferrara, Italy*
[11] *Istituto Nazionale di Fisica Nucleare, Laboratori Nazionali di Frascati, 00044 Frascati, Italy*
[12] *Department of Physics, Florida International University, Miami, Florida 33199, USA*
[13] *Fakultät für Physik, Universität Freiburg, 79104 Freiburg, Germany*
[14] *Department of Subatomic and Radiation Physics, University of Gent, 9000 Gent, Belgium*
[15] *Max-Planck-Institut für Kernphysik, 69029 Heidelberg, Germany*
[16] *Department of Physics, University of Illinois, Urbana, Illinois 61801, USA*
[17] *Department of Physics and Astronomy, University of Kentucky, Lexington, Kentucky 40506,USA*
[18] *Physics Department, University of Liverpool, Liverpool L69 7ZE, United Kingdom*
[19] *Department of Physics, University of Wisconsin-Madison, Madison, Wisconsin 53706, USA*
[20] *Physikalisches Institut, Philipps-Universität Marburg, 35037 Marburg, Germany*

[21] *Laboratory for Nuclear Science, Massachusetts Institute of Technology, Cambridge, Massachusetts 02139, USA*
[22] *Randall Laboratory of Physics, University of Michigan, Ann Arbor, Michigan 48109-1120, USA*
[23] *Lebedev Physical Institute, 117924 Moscow, Russia*
[24] *Sektion Physik, Universität München, 85748 Garching, Germany*
[25] *Department of Physics, New Mexico State University, Las Cruces, New Mexico 88003, USA*
[26] *Nationaal Instituut voor Kernfysica en Hoge-Energiefysica (NIKHEF), 1009 DB Amsterdam, The Netherlands*
[27] *Physics Department, Oregon State University, Corvallis, Oregon 97331, USA*
[28] *Department of Physics and Astronomy, University of Pennsylvania, Philadelphia, Pennsylvania 19104-6396, USA*
[29] *Petersburg Nuclear Physics Institute, St. Petersburg, 188350 Russia*
[30] *Institut für Theoretische Physik, Universität Regensburg, 93040 Regensburg, Germany*
[31] *Istituto Nazionale di Fisica Nucleare, Sezione Sanità and Physics Laboratory, Istituto Superiore di Sanità, 00161 Roma, Italy*
[32] *Department of Physics, Simon Fraser University, Burnaby, British Columbia V5A 1S6, Canada*
[33] *TRIUMF, Vancouver, British Columbia V6T 2A3, Canada*
[34] *Department of Physics, Tokyo Institute of Technology, Tokyo 152, Japan*
[35] *Department of Physics and Astronomy, Vrije Universiteit, 1081 HV Amsterdam, The Netherlands*
[36] *Yerevan Physics Institute, 375036, Yerevan, Armenia*

Spin asymmetries of semi-inclusive cross sections for the production of positively and negatively charged hadrons have been measured in deep-inelastic scattering of polarized positrons on polarized hydrogen and ^{3}He targets, in the kinematic range $0.023 < x < 0.6$ and 1 GeV$^2 < Q^2 < 10$ GeV^2. Polarized quark distributions are extracted as a function of x for up $(u+\bar{u})$ and down $(d+\bar{d})$ flavors. The up quark polarization is positive and the down quark polarization is negative in the measured range. The polarization of the sea is compatible with zero. The first moments of the polarized quark distributions are presented. The isospin non-singlet combination Δq_3 is consistent with the prediction based on the Bjorken sum rule. The moments of the polarized quark distributions are compared to predictions based on SU(3)$_f$ flavor symmetry and to a prediction from lattice QCD.

The understanding of the spin structure of the nucleon in terms of quarks and gluons remains a challenge since it was demonstrated by EMC [1] and later experiments [2–13] using inclusive deep-inelastic scattering (DIS) that only a fraction of the nucleon spin can be attributed to the quark spins and that the strange quark sea seems to be negatively polarized [14]. These conclusions follow from the extraction of the first moments of up, down and strange quark spin distributions from the inclusive data by assuming SU(3)$_f$ flavor symmetry. With semi-inclusive polarized deep-inelastic scattering experiments, the separate spin contributions Δq_f of quark and antiquark flavors f to the total spin of the nucleon can be determined as a function of the Bjorken scaling variable x. Semi-inclusive data can be used to measure the sea polarization directly and to test SU(3)$_f$ symmetry by comparing the first moments of the flavor distributions to the SU(3)$_f$ predictions.

Hadron production in DIS is described by the absorption of a virtual photon by a point-like quark and the subsequent fragmentation into a hadronic final state. The two processes can be characterized by two functions: the quark distribution function $q_f(x, Q^2)$, and the fragmentation function $D_f^h(z, Q^2)$. The semi-inclusive DIS cross section $\sigma^h(x, Q^2, z)$ to produce a hadron of type h with energy fraction $z = E_h/\nu$ is then given by

$$\sigma^h(x, Q^2, z) \propto \sum_f e_f^2 q_f(x, Q^2) D_f^h(z, Q^2). \quad (1)$$

The sum is over quark and antiquark types $f =$

$(u, \bar{u}, d, \bar{d}, s, \bar{s})$. In the target rest frame, E_h is the energy of the hadron, $\nu = E - E'$ and $-Q^2$ are the energy and the squared four-momentum of the exchanged virtual photon, $E(E')$ is the energy of the incoming (scattered) lepton and e_f is the quark charge in units of the elementary charge. The Bjorken variable x is calculated from the kinematics of the scattered lepton according to $x = Q^2/2M\nu$ with M being the nucleon mass. It is assumed that the fragmentation process is spin independent, i.e. that the probability to produce a hadron of type h from a quark of flavor f is independent of the relative spin orientations of quark and nucleon. The spin asymmetry A_1^h in the semi-inclusive cross section for production of a hadron of type h by a polarized virtual photon is given by

$$A_1^h(x, Q^2, z) = \frac{\sum_f e_f^2 \Delta q_f(x, Q^2) D_f^h(z, Q^2)}{\sum_f e_f^2 q_f(x, Q^2) D_f^h(z, Q^2)} \frac{(1 + R(x, Q^2))}{(1 + \gamma^2)}$$

$$(2)$$

where $\Delta q_f(x, Q^2) = q_f^{\uparrow\uparrow}(x, Q^2) - q_f^{\uparrow\downarrow}(x, Q^2)$ is the polarized quark distribution function and $q_f^{\uparrow\uparrow(\uparrow\downarrow)}(x, Q^2)$ is the distribution function of quarks with spin orientation parallel (anti-parallel) to the spin of the nucleon. The ratio $R = \sigma_L/\sigma_T$ of the longitudinal to transverse photon absorption cross sections appears in this formula to correct for the longitudinal component that is included in the experimentally determined parametrizations of $q_f(x, Q^2)$ but not in $\Delta q_f(x, Q^2)$. It is assumed that the ratio of

longitudinal to transverse components is flavor and target independent and that the contribution from the second spin structure function $g_2(x, Q^2)$ can be neglected. The term $\gamma = \sqrt{Q^2}/\nu$ is a kinematic factor. Eq. (2) can be used to extract the quark polarizations $\Delta q_f(x)/q_f(x)$ from a set of measured asymmetries on the proton and neutron for positively and negatively charged hadrons.

This paper reports on the extraction of polarized quark distribution functions from data taken by the HERMES experiment [15] using the 27.5 GeV beam of longitudinally polarized positrons in the HERA storage ring at DESY, incident on a longitudinally polarized ^{3}He or ^{1}H internal gas target.

The positron beam at HERA becomes transversely polarized by synchrotron radiation emission through its asymmetric spin-flip probabilities [16]. The required longitudinal polarization direction at the HERMES experiment is obtained using spin rotators located upstream and downstream of the experiment [17]. The beam polarization is measured continuously using Compton backscattering of circularly polarized laser light [18,19]. The average polarization for the analyzed data was 0.55. The fractional statistical error for a single 60 s polarization measurement was typically 1-2% and the overall fractional systematic error was 4.0% (3.4%) for the ^{3}He (H) measurement, dominated by the uncertainty in the calibration of the beam polarimeters.

The internal target consists of polarized ^{3}He (H) gas confined in a storage cell [20], which is a 400 mm long open-ended thin-walled elliptical tube mounted coaxially with the HERA positron beam. It was fed by an optically pumped source of polarized ^{3}He atoms [21] in 1995, and by an atomic beam source of nuclear-polarized hydrogen based on Stern-Gerlach separation [22] in 1996 and 1997. The tube was constructed of 125 μm (75 μm) thick ultra-pure aluminum and was cooled to typically 25 K (100 K) [21]. This provided a target with an areal density of approximately 3.3×10^{14} ^{3}He-atoms/cm^2 (7×10^{13} H-atoms/cm^2). During H operation, a drifilm-coated cell [23] was used to minimize wall collision effects. There is good evidence that recombination is further suppressed by water deposited on the cell surface during normal operation [20]. The polarization direction was defined by a 3.5 mT (335 mT) magnetic field parallel to the beam direction and was reversed every 10 (1-2) minutes. The polarizations of the ^{3}He gas in both the pumping and the storage cell were measured continuously with optical polarimeters. The average ^{3}He target polarization was 0.46 with a fractional uncertainty of 5%. The relative populations of the hydrogen atomic states were measured in a Breit-Rabi polarimeter [24]. A target gas analyser was used to measure the atomic and the molecular content of the hydrogen gas. The average proton target polarization was 0.86 with a fractional uncertainty of 5%. The luminosity was measured by detecting Bhabha-scattered target electrons in coincidence with the scattered positron.

During the course of a positron fill of typically 8 hours, the current in the ring decreased from typically 40 mA at injection to about 10 mA.

The HERMES detector is an open-geometry forward spectrometer. A detailed description is given in Ref. [25]. The geometrical acceptance of $\pm$(40-140) mrad in the vertical direction and $\pm$170 mrad in the horizontal direction allows detection of hadrons produced in coincidence with the scattered lepton. The DIS trigger is formed from a coincidence between signals in scintillator hodoscope planes and a lead-glass calorimeter. The identification of the scattered lepton is accomplished using the calorimeter, a preshower counter, a transition radiation detector, and a gas threshold Čerenkov counter. This system provides positron identification with an average efficiency of 98% and a hadron contamination of less than 1%. The threshold Čerenkov counter provides pion identification in a limited kinematic range.

Polarized quark distributions have been extracted from a combination of inclusive and semi-inclusive asymmetry data on ^{3}He and hydrogen. As the wave function for ^{3}He is dominated by the configuration with the two protons paired to zero spin, most of the asymmetry from ^{3}He is due to the neutron [26]. The analysis procedure described in Ref. [12,13,27,28] was applied. The inclusive (semi-inclusive) asymmetry $A_1^{(h)}$ was extracted from the measured asymmetry $A_\parallel^{(h)}$ using the relation

$$A_1^{(h)} = A_\parallel^{(h)} / \left[D(1 + \gamma\eta) \right] , \qquad (3)$$

where D is the depolarization factor for the virtual photon and η is a kinematic factor as given in Ref. [13]. In Eq. (3) the approximation is used that the contribution of the second spin structure function g_2 to $A_1^{(h)}$ can be neglected. In the kinematic region of our measurement g_2 was previously measured to be consistent with zero for the proton and neutron [29,30]. In each kinematic bin the value of $A_\parallel^{(h)}$ was extracted from the measured counting rates using

$$A_\parallel^{(h)} = \frac{N_{(h)}^{\uparrow\downarrow} L^{\uparrow\uparrow} - N_{(h)}^{\uparrow\uparrow} L^{\uparrow\downarrow}}{N_{(h)}^{\uparrow\downarrow} L_P^{\uparrow\uparrow} + N_{(h)}^{\uparrow\uparrow} L_P^{\uparrow\downarrow}} , \qquad (4)$$

where $N^{\uparrow\uparrow}$ ($N^{\uparrow\downarrow}$) are the numbers of DIS events for target polarization parallel (anti-parallel) to the beam polarization, and $N_h^{\uparrow\uparrow}$ ($N_h^{\uparrow\downarrow}$) are the corresponding numbers of hadrons in coincidence with a DIS event. Here, $L^{\uparrow\uparrow(\uparrow\downarrow)}$ are the luminosities for each spin state corrected for dead time, and $L_P^{\uparrow\uparrow(\uparrow\downarrow)}$ are the luminosities corrected for dead time and weighted by the product of beam and target polarizations for each spin state.

After applying data quality criteria and kinematic requirements to select DIS events ($Q^2 > 1$ GeV^2, $W^2 > 4$ GeV^2 and $y < 0.85$), 2.2×10^6 (2.3×10^6)
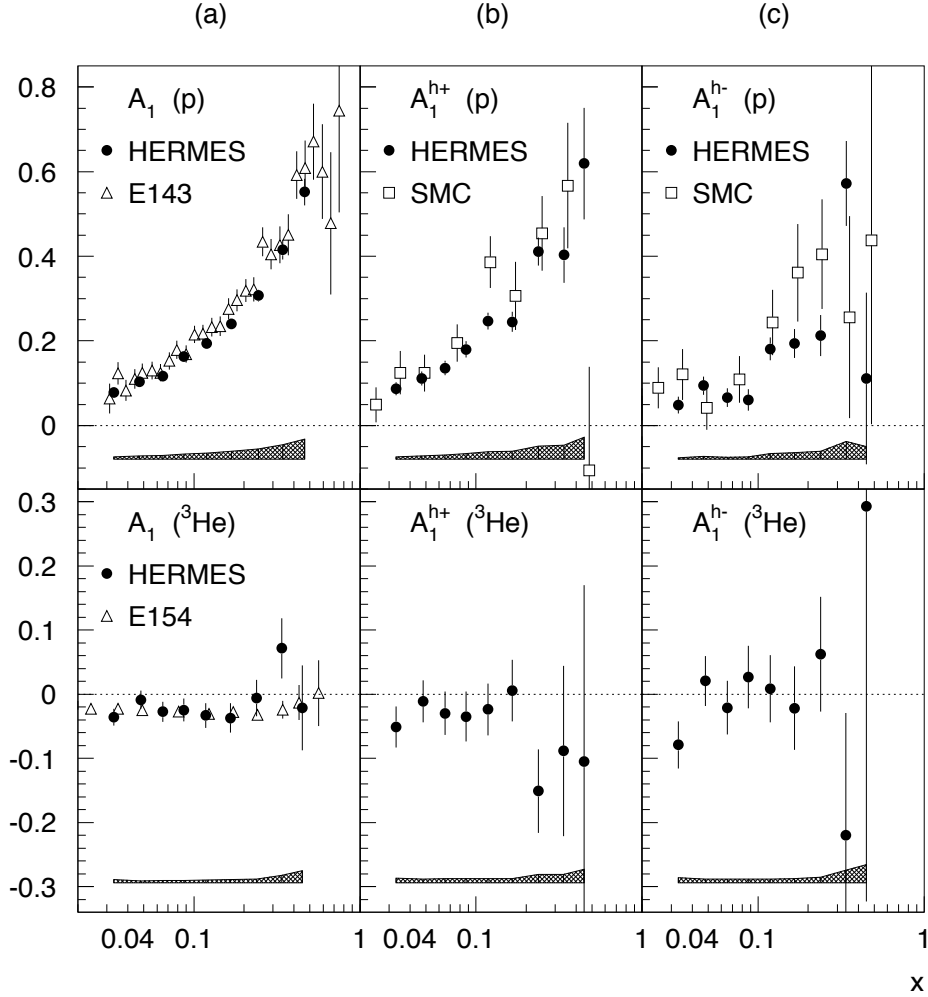
FIG. 1. The inclusive (a) and semi-inclusive asymmetries for positively (b) and negatively (c) charged hadrons on the proton (top) and ^{3}He (bottom) target. The inclusive asymmetries are compared to SLAC results for g_1/F_1 (open triangles). The hadron asymmetries on the proton are compared to SMC results (open squares) truncated to the HERMES x-range. The data points are given for the measured mean Q^2 at each value of x, which is different for the different experiments. The error bars of the HERMES (SLAC and SMC) data are statistical (total) uncertainties and the bands are systematic uncertainties of the HERMES data.

events were available for analysis on ^{3}He (H). Here, $y = \nu/E$ is the fractional energy transfer to the virtual photon and W is the invariant mass of the initial photon-nucleon system. The data cover the ranges $0.023 < x < 0.6$ and 1 GeV$^2 < Q^2 < 10$ GeV^2. For the semi-inclusive asymmetries, the hadrons containing information on the struck quark were distinguished from target region fragments by requiring each hadron to have a minimum z of 0.2 and $x_F \approx 2p_L/W$ of 0.1, where p_L is the longitudinal momentum of the hadron with respect to the virtual photon in the photon-nucleon center of mass frame. A minimum W^2 cut of 10 GeV^2 was additionally imposed for these events to improve the separation between the current and target fragmentation regions. After applying all cuts, 284×10^3 (306×10^3) positive

and 178×10^3 (175×10^3) negative hadrons remained for the ^{3}He (H) target. Small corrections were applied to account for charge symmetric background processes (e.g. $\gamma \to e^+e^-$). Smearing corrections were applied to all data and QED radiative corrections were applied only to the inclusive asymmetries, but not to the semi-inclusive asymmetries, where the corrections are negligible [31,32].

The dominant sources of systematic uncertainties in the measured asymmetries are: the target and beam polarization measurements, the uncertainty assigned for observed yield fluctuations in the ^{3}He data [12] and the systematic uncertainty on R [13]. By averaging over data taken with opposite beam helicities, a possible instrumental bias is further reduced. Fig. 1 shows the extracted inclusive asymmetries and the

semi-inclusive asymmetries for positively and negatively charged hadrons on both targets. The measured spin asymmetries $A_1^h(x, Q^2, z)$ were integrated in each x bin over the corresponding Q^2-range and the z-range from 0.2 to 1 to yield $A_1^h(x)$. Also shown are inclusive results measured at a similar energy at SLAC [5,6,29,33] and hadron asymmetries on hydrogen measured by SMC [34]. The data are in agreement within the quoted uncertainties. The agreement of the HERMES data with the SMC data, taken at 6-12 times higher average Q^2, shows that the semi-inclusive asymmetries are Q^2 independent within the present accuracy of the experiments.

Eq. (2) is used to extract polarized quark distribution functions from semi-inclusive asymmetries. It can be written as

$$A_1^h(x) = \sum_f P_f^h(x) \frac{\Delta q_f(x)}{q_f(x)} \frac{(1 + R(x))}{(1 + \gamma^2)} \qquad (5)$$

where $P_f^h(x)$ are the integrated purities [28,35] defined as

$$P_f^h(x) = \frac{e_f^2 q_f(x) \int_{0.2}^1 D_f^h(z)\, dz}{\sum_{f'} e_{f'}^2 q_{f'}(x) \int_{0.2}^1 D_{f'}^h(z')\, dz'}. \qquad (6)$$

The inclusive asymmetry A_1 is similarly expressed by replacing P_f^h by P_f where $P_f(x) = e_f^2 q_f(x)/\sum_{f'} e_{f'}^2 q_{f'}(x)$. After integrating over z, Eq. (5) together with the corresponding inclusive case can be written in matrix form

$$\vec{A}(x) = \mathcal{P}(x) \cdot \vec{Q}(x) \qquad (7)$$

where the vector $\vec{A} = (A_{1p}, A_{1p}^{h^+}, A_{1p}^{h^-}, A_{1He}, A_{1He}^{h^+}, A_{1He}^{h^-})$ contains as elements the measured asymmetries. The vector $\vec{Q}(x)$ contains the quark and antiquark polarizations. The matrix $\mathcal{P}$ contains the effective integrated purities for the proton and ^{3}He as well as the $(1+R)/(1+\gamma^2)$ factor. These purities describe the probability that the virtual photon hit a quark of flavor f when a hadron of type h is detected in the experiment. They include the effects of the acceptance of the experiment and have been determined with a Monte Carlo simulation using the LUND string fragmentation model [36], a model of the detector, the CTEQ Low–Q^2 parametrizations [37] for the unpolarized parton distributions and values for R from Ref. [38]. The LUND fragmentation parameters were tuned to fit the measured hadron multiplicities. For the ^{3}He data, a correction was applied for the non-zero polarization of the protons of -0.028 ± 0.004 and the neutron polarization of 0.86 ± 0.02 [39]. Eq. (7) can be solved for $\vec{Q}(x)$ by minimizing

$$\chi^2 = \left(\vec{A} - \mathcal{P} \cdot \vec{Q}\right)^{\mathrm{T}} \mathcal{V}_{\vec{A}}^{-1} \left(\vec{A} - \mathcal{P} \cdot \vec{Q}\right). \qquad (8)$$

where $\mathcal{V}_{\vec{A}}$ is the covariance matrix of the asymmetry vector $\vec{A}$. In the fit procedure constraints were imposed on

the sea polarization to improve statistical significance. In view of rather ambiguous theoretical model predictions [40,41], two alternatives were chosen for relating the spin distributions of the sea flavors. As a first possibility it was assumed that the polarization $\Delta q_s(x)/q_s(x)$ of sea quarks is independent of flavor:

$$\frac{\Delta u_s(x)}{u_s(x)} = \frac{\Delta d_s(x)}{d_s(x)} = \frac{\Delta s(x)}{s(x)} = \frac{\Delta \bar{u}(x)}{\bar{u}(x)} = \frac{\Delta \bar{d}(x)}{\bar{d}(x)} = \frac{\Delta \bar{s}(x)}{\bar{s}(x)}. \qquad (9)$$

This approach is used for all calculations unless otherwise stated. As a second approach, a pure singlet spin distribution of the sea is considered:

$$\Delta u_s(x) = \Delta d_s(x) = \Delta s(x) = \Delta \bar{u}(x) = \Delta \bar{d}(x) = \Delta \bar{s}(x). \qquad (10)$$

The flavor decomposition is obtained by solving Eq. (7) for a vector $\vec{Q}$, which contains the sum of quarks and antiquarks

$$\vec{Q} = \left(\frac{\Delta u(x) + \Delta \bar{u}(x)}{u(x) + \bar{u}(x)}, \frac{\Delta d(x) + \Delta \bar{d}(x)}{d(x) + \bar{d}(x)}, \frac{\Delta s(x) + \Delta \bar{s}(x)}{s(x) + \bar{s}(x)}\right), \qquad (11)$$

where due to assumption (9) the polarizations of the strange quarks and of the total sea are equal: $(\Delta s(x) + \Delta \bar{s}(x))/(s(x) + \bar{s}(x)) = \Delta q_s(x)/q_s(x)$. For $x > 0.3$ the sea polarization is set to zero and the corresponding effect on the results for the non-sea polarizations is included in their systematic uncertainties. Fig. 2 shows the results. The up quark polarizations are positive and the down quark polarizations are negative over the measured range of x. Their absolute values are largest at large x and remain different from zero in the sea region. The sea polarization is compatible with zero over the measured range of x. The overall χ^2 per degree of freedom of the fit is 1.1.

The systematic uncertainties, shown by the shaded band in Fig. 2, were determined from the uncertainties on the measured asymmetries, the unpolarized parton distributions and the purities. The uncertainty on the unpolarized parton distributions was derived by comparing different parametrizations [37,42] of the world data. The uncertainty coming from the symmetry assumption of the sea polarization was derived by comparing the results produced by Eqs. (9) and (10) respectively. The fitted quark polarizations change by typically less than 0.01 when the assumption in Eq. (9) is replaced by (10). The uncertainty in the purities was determined by comparing different fragmentation models [43,44] and varying the fragmentation parameters in the Monte Carlo code.
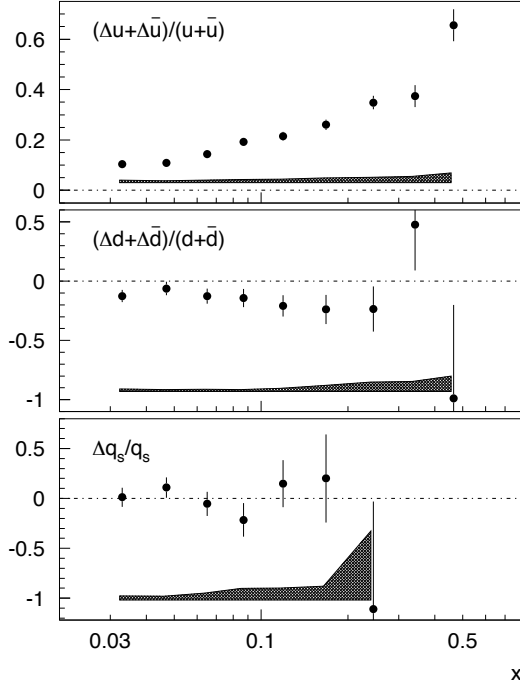
FIG. 2. The flavor decomposition $(\Delta u(x) + \Delta \bar{u}(x))/$ $(u(x)+\bar{u}(x))$, $(\Delta d(x)+\Delta\bar{d}(x))/(d(x)+\bar{d}(x))$ and $\Delta q_s(x)/q_s(x)$ of the quark polarization as a function of x, derived from the HERMES inclusive and semi-inclusive asymmetries. The sea polarization is assumed to be flavor symmetric in this analysis. The error bars shown are the statistical and the bands represent the systematic uncertainties.

The polarized quark distributions $\Delta q_f(x)$ were determined by forming the products of the polarizations $\Delta q_f(x)/q_f(x)$ and the unpolarized parton distributions from Ref. [37] at $Q^2 = 2.5$ GeV^2. It was assumed that the polarization is independent of Q^2 within the Q^2 range of this measurement. This assumption is justified by the weak Q^2 dependence predicted by QCD and by the experimental result that there is no significant Q^2 dependence observed in the inclusive asymmetries (see e.g. Ref. [13]) and in the semi-inclusive asymmetries as shown in Fig. 1. The results for the up and down distributions are shown in Fig. 3 and compared with different sets of parametrizations of world data in leading order QCD [45–47]. Parametrizations that were fitted to spin asymmetries A_1 under the assumption $R = 0$ do not fit the HERMES data for $x(\Delta u(x) + \Delta \bar{u}(x))$. They can be brought into agreement with the HERMES results by dividing by $1 + R$. Fig. 3 demonstrates the size of the effect for the parametrization by Glück et al.. Parametrizations that are derived from fits to g_1 instead of A_1 (e.g. Gehrmann and Stirling) do not need this correction.

The upper plots in Fig. 4 show the polarized valence quark distributions $x\Delta u_v(x)$ and $x\Delta d_v(x)$, derived from the relation $\Delta q_v(x) = (\Delta q(x) + \Delta\bar{q}(x)) - 2\Delta\bar{q}(x)$. Since
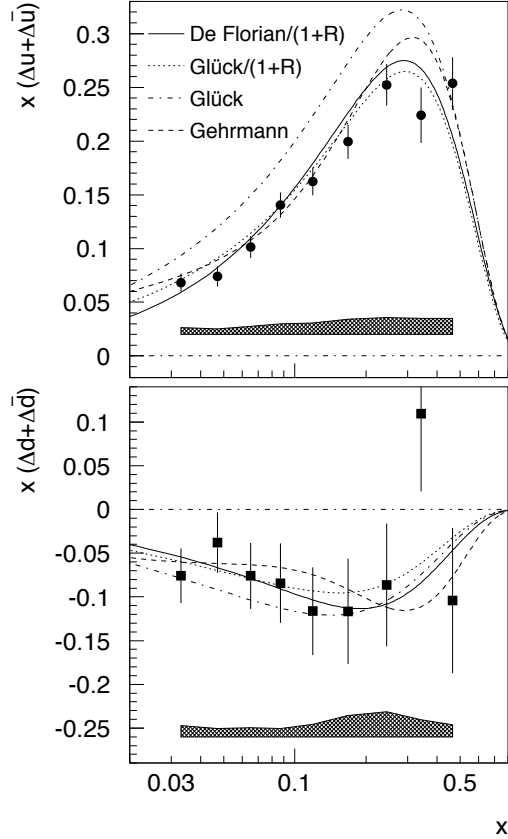

FIG. 3. The quark spin distributions at $Q^2 = 2.5$ GeV^2 separately for $x(\Delta u(x) + \Delta \bar{u}(x))$ and $x(\Delta d(x) + \Delta \bar{d}(x))$ as a function of x. They are compared to different sets of parametrizations which correspond to the following publications: De Florian et al. ($0.1 < \Delta G < 0.8$, LO) [45], Gehrmann and Stirling ('Gluon A', LO) [46], and Glück et al. ('Standard Scenario', LO) [47]. The De Florian and Glück parametrizations are corrected by a factor $(1 + R)$ to allow for a direct comparison. The error bars shown are the statistical and the bands represent the systematic uncertainties.

for scattering off sea quarks the contribution from u_s and $\bar{u}$ quarks dominates, the polarized $x\Delta\bar{u}(x)$ sea distribution is shown in the lower plot. Fig. 4 includes results from SMC [34] obtained at $Q^2 = 10$ GeV^2, which are shown here for the x-range explored by HERMES and which are extrapolated to $Q^2 = 2.5$ GeV^2 by assuming a Q^2-independent polarization $\Delta q(x)/q(x)$. The SMC results are derived under the assumption presented in Eq. (10) rather than (9). The positivity limit and a parametrization of data from Ref. [46] are included in Fig. 4. The parametrization and the SMC results are consistent with the HERMES results within the statistical and systematic uncertainties. The uncertainties of the
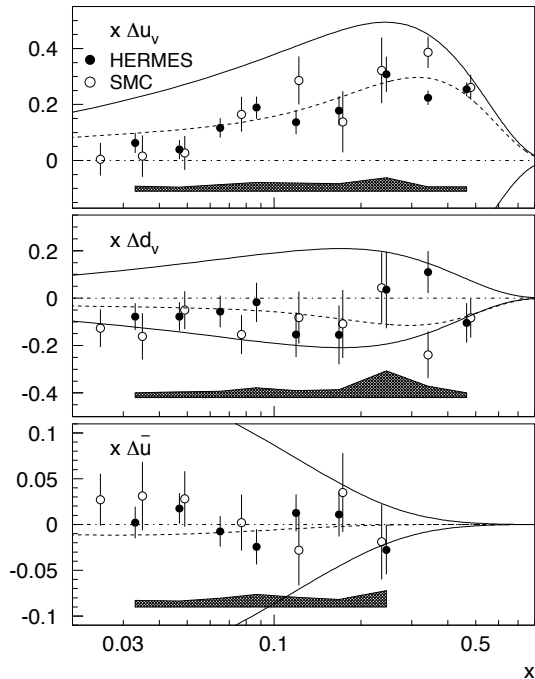
FIG. 4. The spin distributions at $Q^2 = 2.5$ GeV^2 separately for the valence quarks $x\Delta u_v(x)$, $x\Delta d_v(x)$ and the sea quarks $x\Delta\bar{u}(x)$ as a function of x. The error bars shown are the statistical and the bands the systematic uncertainties. The distributions are compared to results from SMC, extrapolated to $Q^2 = 2.5$ GeV^2. The error bars of the SMC result correspond to its total uncertainty. The solid lines indicate the positivity limit and the dashed lines are the parametrization from Gehrmann and Stirling ('Gluon A', LO) [46].

HERMES data for $x\Delta u_v(x)$ and $x\Delta\bar{u}(x)$ are much smaller than for the SMC data.

In the quark parton model the isospin non-singlet combination $\Delta q^{NS}(x) = \Delta u(x) + \Delta\bar{u}(x) - \Delta d(x) - \Delta\bar{d}(x)$ is directly related to the spin structure functions according to $\Delta q^{NS}(x) = 6(g_1^p(x) - g_1^n(x))$. Fig. 5 illustrates that the HERMES result for $\Delta q^{NS}(x)$ is in good agreement with parametrizations of other published inclusive data.

The first and second moments of spin distributions have been calculated and compared to other experimental data and to model predictions. In the measured x-region, the integral Δq_f is obtained as

$$\Delta q_f = \sum_i \left(\left.\frac{\Delta q_f}{q_f}\right|_i \int_{x_i}^{x_{i+1}} q_f(x)\, dx \right), \qquad (12)$$

where $(\Delta q_f/q_f)|_i$ is constant within each bin (x_i, x_{i+1}) and $q_f(x)$ is a parametrization given in Ref. [37]. Outside the measured region $0.023 < x < 0.6$, extrapolations are required. There is no clear prediction for the low-x
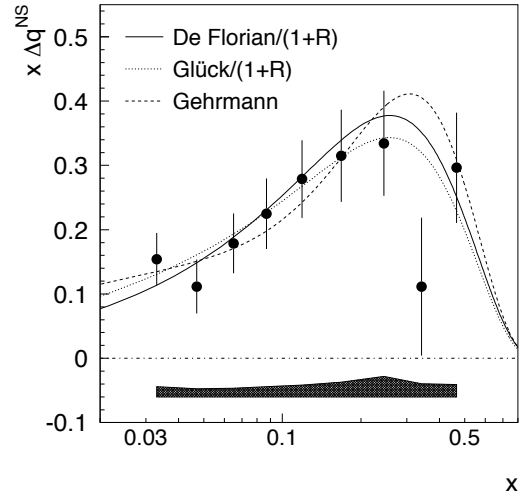

FIG. 5. The non-singlet contribution $x\Delta q^{NS}(x)$ at $Q^2 = 2.5$ GeV^2. The result is compared to the same sets of parametrizations as in Figure 3. The error bars are the statistical and the band the systematic uncertainties.

extrapolation [6]. For comparison with previous measurements we quote the integrals assuming a simple Regge parametrization [48,49] of $\Delta q_f(x) \propto x^{-\alpha}$ with $\alpha = 0$ fitted to the data for $x < 0.075$. Due to the strong model dependence of the result, no error is quoted for the extrapolation. The extrapolation to $x = 1$ was obtained by fitting the functional form from Ref. [47] to our data. The fit is constrained to fulfill the positivity limit $|\Delta q_f(x)/q_f(x)| \leq (1+\gamma^2)/(1+R(x))$. The systematic uncertainty of the high-x extrapolation is small and included in the quoted uncertainty of the total integral.

The results are listed in Table I. The spin carried by up, down and strange quarks is compared to results from the $SU(3)_f$ analysis of the inclusive data. The comparison is performed by using the Δq_0 value and the QCD corrections from Ref. [14]. We obtain values for the up, down and strange contributions which differ from our semi-inclusive result. The sea quark contribution is found to be close to zero in this semi-inclusive analysis whereas the strange quark sea is significantly negative in the inclusive analysis. Neither result represents a direct measurement of the strange spin distribution but rather depends on the assumptions of $SU(3)_f$ symmetry for the inclusive case and on the sea symmetry condition (Eq. (9)) for the semi-inclusive case. To interpret the differences that are observed in the contributions from up and down quarks, the flavor distributions have been separated into $SU(3)_f$ singlet (Δq_0), triplet (Δq_3), and octet (Δq_8) contributions, as shown in Table I. The total spin integral

7

TABLE I. The integrals of various spin distributions. The results are given for the measured region $0.023 < x < 0.6$, for the low-x extrapolation and for the total integral. Note that the entry for $\Delta s + \Delta \bar{s}$ does not represent a direct measurement of the strange sea but relies on the assumption in Eq. (9) (see text). An uncertainty of the Regge-type extrapolation at low-x is not included in the quoted error for the total integral. The items $x\Delta u_v$ and $x\Delta d_v$ denote the second moments. Δq_8^* uses Eq. (10) whereas all other quantities use Eq. (9) as symmetry condition. The HERMES results are given for $Q^2 = 2.5$ GeV^2. The Q^2 values of the predictions are quoted in GeV^2.

	measured region	low-x	total integral	prediction		Q^2
$\Delta u + \Delta \bar{u}$	$0.51 \pm 0.02 \pm 0.03$	0.04	$0.57 \pm 0.02 \pm 0.03$	0.66 ± 0.03	SU(3)	2.5
$\Delta d + \Delta \bar{d}$	$-0.22 \pm 0.06 \pm 0.05$	-0.03	$-0.25 \pm 0.06 \pm 0.05$	-0.35 ± 0.03	SU(3)	2.5
$\Delta s + \Delta \bar{s}$	$-0.01 \pm 0.03 \pm 0.04$	0.00	$-0.01 \pm 0.03 \pm 0.04$	-0.08 ± 0.02	SU(3)	2.5
$\Delta \bar{u}$	$-0.01 \pm 0.02 \pm 0.03$	0.00	$-0.01 \pm 0.02 \pm 0.03$			
$\Delta \bar{d}$	$-0.02 \pm 0.03 \pm 0.04$	0.00	$-0.01 \pm 0.03 \pm 0.04$			
Δq_0	$0.28 \pm 0.04 \pm 0.09$	0.01	$0.30 \pm 0.04 \pm 0.09$	0.23 ± 0.04	SU(3) [14]	2.5
Δq_3	$0.74 \pm 0.07 \pm 0.06$	0.07	$0.84 \pm 0.07 \pm 0.06$	1.01 ± 0.05	Bjorken	2.5
Δq_8	$0.32 \pm 0.09 \pm 0.10$	0.01	$0.32 \pm 0.09 \pm 0.10$	0.35 ± 0.07	non-SU(3) [58]	2.5
Δq_8^*	$0.33 \pm 0.10 \pm 0.11$	0.00	$0.33 \pm 0.10 \pm 0.11$	0.46 ± 0.03	$F\&D$	2.5
Δu_v	$0.52 \pm 0.05 \pm 0.08$	0.03	$0.57 \pm 0.05 \pm 0.08$	0.84 ± 0.05	Lattice [59]	5
Δd_v	$-0.19 \pm 0.11 \pm 0.13$	-0.03	$-0.22 \pm 0.11 \pm 0.13$	-0.25 ± 0.02	Lattice [59]	5
$x\Delta u_v$	$0.12 \pm 0.01 \pm 0.01$	0.00	$0.13 \pm 0.01 \pm 0.01$	0.198 ± 0.008	Lattice [59]	4
$x\Delta d_v$	$-0.02 \pm 0.02 \pm 0.02$	0.00	$-0.02 \pm 0.02 \pm 0.02$	-0.048 ± 0.003	Lattice [59]	4

$\Delta q_0 = \int_0^1 (\Delta u(x) + \Delta \bar{u}(x) + \Delta d(x) + \Delta \bar{d}(x) + \Delta s(x) + \Delta \bar{s}(x))\, dx = 0.23 \pm 0.04$ agrees well with the HERMES result $0.30 \pm 0.04(stat.) \pm 0.09(syst.)$. The large theoretical uncertainties on the extrapolation at low x are not included here. The triplet contribution $\Delta q_3 = \int_0^1 \Delta q^{NS}(x)\, dx = 0.84 \pm 0.07(stat.) \pm 0.06(syst.)$ is directly related to the Bjorken sum rule [50] according to

$$\int_0^1 \Delta q^{NS}(x)\, dx = \left| \frac{g_a}{g_v} \right| \times C_{\text{QCD}} \qquad (13)$$

with the QCD correction C_{QCD} according to Ref. [14,51,52]. Higher twist corrections are expected to be small [53–56] and have been neglected. The semi-inclusive result agrees with the prediction of the Bjorken sum rule of 1.01 ± 0.05 obtained including an estimate of the QCD correction in 4th order in $\alpha_s = 0.35 \pm 0.04$ for $Q^2 = 2.5$ GeV^2. The large theoretical error of the Bjorken sum rule prediction comes from the uncertainties in α_s.

The Ellis-Jaffe sum rule [57], which is based on SU(3)$_f$ flavor symmetry and on the assumption of a zero polarization of strange quarks, has been found to be violated [1–13]. Models to explain this discrepancy invoke either SU(3)$_f$ symmetry breaking, a large negative strange quark polarization, or SU(3)$_f$-asymmetric polarized sea distributions. Semi-inclusive data provide a test of such models. This is illustrated for two examples: (i) a model with symmetric sea (Eq. (10)) and unbroken SU(3)$_f$ and (ii) a model which is not SU(3)$_f$ symmetric combined with a flavor asymmetric sea according to Eq. (9).

In the first case the octet combination $\Delta q_8 =$

$\int_0^1 (\Delta u(x) + \Delta \bar{u}(x) + \Delta d(x) + \Delta \bar{d}(x) - 2(\Delta s(x) + \Delta \bar{s}(x)))\, dx$ can be related to the hyperon decay constants F and D according to $\Delta q_8 = (3F - D) \times C_{\text{QCD}} = 0.46 \pm 0.03$, where C_{QCD} is taken from Ref. [52]. The semi-inclusive result yields $\Delta q_8 = 0.33 \pm 0.10(stat.) \pm 0.11(syst.)$ which is lower than the prediction, but still consistent.

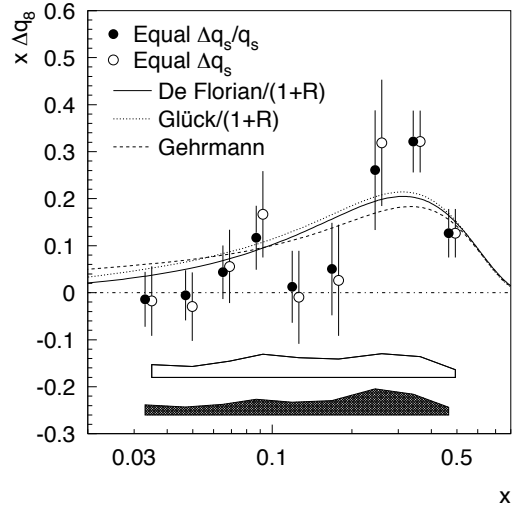FIG. 6. The SU(3)$_f$ octet combination $x\Delta q_8(x)$ at $Q^2 = 2.5$ GeV^2 assuming a flavor symmetric sea (open circles) or a flavor independent polarization (full circles). The data are compared to the same sets of parametrizations as in Figure 3. The error bars shown are the statistical and the upper (lower) band shows the systematic uncertainties which correspond to the open (full) circles.

TABLE II. Comparison of the HERMES integrals of valence and sea spin distributions with SMC results. The SMC values are extrapolated to $Q^2 = 2.5$ GeV^2 and integrated over the HERMES x-range of $0.023 < x < 0.6$.

	HERMES	SMC
$\Delta\bar{u}$	$-0.01 \pm 0.02 \pm 0.03$	$0.02 \pm 0.03 \pm 0.02$
$\Delta\bar{d}$	$-0.02 \pm 0.03 \pm 0.04$	$0.02 \pm 0.03 \pm 0.02$
Δu_v	$0.52 \pm 0.05 \pm 0.08$	$0.59 \pm 0.08 \pm 0.07$
Δd_v	$-0.19 \pm 0.11 \pm 0.13$	$-0.33 \pm 0.11 \pm 0.09$
$x\Delta u_v$	$0.12 \pm 0.01 \pm 0.01$	$0.15 \pm 0.02 \pm 0.01$
$x\Delta d_v$	$-0.02 \pm 0.02 \pm 0.02$	$-0.05 \pm 0.02 \pm 0.02$

A similar deviation shows up at low x in the comparison of the semi-inclusive result of $\Delta q_8(x)$ with the fits from Ref. [45–47] which are dominated by inclusive data (see Fig. 6).

In the second case we assume a flavor asymmetric polarized sea according to Eq. (9) and obtain from the semi-inclusive analysis the result $\Delta q_8 = 0.32 \pm 0.09(stat.) \pm 0.10(syst.)$. Following Ref. [58] Δq_8 can be calculated according to

$$\Delta q_8 = \frac{2\epsilon\Delta q_0 + 3(3F - D)C_{\text{QCD}}}{3 + 2\epsilon} \qquad (14)$$

where ϵ is estimated from the averaged ratio of distribution functions in Ref. [37] according to $1 + \epsilon = \langle\Delta\bar{d}(x)/\Delta\bar{s}(x)\rangle = \langle\bar{d}(x)/\bar{s}(x)\rangle = 4.8 \pm 0.4$. The model yields $\Delta q_8 = 0.35 \pm 0.07$.

The results are compatible with both assumptions and do not allow for a definite statement about the question whether the polarized quark distributions violate SU(3) flavor symmetry. A direct measurement of the strange sea is required for a final conclusion about the reason for the violation of the Ellis-Jaffe sum rule.

The first and second moments of the valence spin distributions $\Delta u_v(x)$ and $\Delta d_v(x)$ have been extracted (see Table I) and are compared to SMC results [34] (see Table II). For this comparison the SMC values have been extrapolated to $Q^2 = 2.5$ GeV^2 and integrated according to Eq. (12) in the HERMES x-range. There is good agreement with the SMC data. Significant deviations are observed between the measured first and second moments of $\Delta u_v(x)$ from predictions by lattice QCD [59]. Notice however, that the QCD calculation has been performed in the quenched approximation. The relative factor between the measured value and the lattice value for the second moment of $\Delta u_v(x)$ is similar to that observed in the unpolarized case [60].

In summary, inclusive and semi-inclusive spin asymmetries on longitudinally polarized hydrogen and ^{3}He targets were measured and used to extract the individual quark spin polarizations for up and down quarks, and for valence and sea quarks. The up distributions are positive, the down distributions are negative and the sea quarks show no significant polarization. The values for the integrals of the polarized quark distributions have

been determined at $Q^2 = 2.5$ GeV^2. The results for the flavor-separated first moments differ from the inclusive results from Ref. [14] that are based on SU(3)$_f$ flavor symmetry. The measured value of the octet combination $\Delta q_8(x)$ is lower but still consistent with the value $3F - D$ predicted by SU(3)$_f$ symmetry arguments. It provides a test for models trying to explain the violation of the Ellis-Jaffe sum rule. The first moment of the non-singlet combination of the polarized quark distributions agrees with predictions from the Bjorken sum rule. Predictions from a quenched lattice QCD calculation overestimate the first and second moments of the polarized valence up quark distribution.

[†] Deceased
[1] EMC, J. Ashman et al., Phys. Lett. B **206** (1988) 364.
[2] E-142, P.L. Anthony et al., Phys. Rev. Lett. **71** (1993) 959.
[3] E-142, P.L. Anthony et al., Phys. Rev. D **54** (1996) 6620.
[4] E-143, K. Abe et al., Phys. Rev. Lett. **75** (1995) 25.
[5] E-143, K. Abe et al., Phys. Rev. Lett. **74** (1995) 346.
[6] E-154, K. Abe et al., Phys. Rev. Lett. **79** (1997) 26.
[7] SMC, B. Adeva et al., Phys. Lett. B **320** (1994) 400.
[8] SMC, D. Adams et al., Phys. Lett. B **396** (1997) 338.
[9] SMC, D. Adams et al., Phys. Lett. B **412** (1997) 414.

[10] SMC, D. Adams *et al.*, Phys. Rev. D **56** (1997) 5330.

[11] SMC, B. Adeva *et al.*, Phys. Rev. D **58** (1998) 112001 and references therein.

[12] HERMES, K. Ackerstaff *et al.*, Phys. Lett. B **404** (1997) 383.

[13] HERMES, A. Airapetian *et al.*, Phys. Lett. B **442** (1998) 484.

[14] J. Ellis and M. Karliner, Phys. Lett. B **341** (1995) 397; J. Ellis and M. Karliner, Invited Lectures at the International School of Nucleon Spin Structure, Erice, August 1995, hep-ph/9601280.

[15] HERMES, K. Coulter *et al.*, *Proposal*, DESY-PRC 90/01 (1990); *Technical Design Report*, DESY-PRC 93/06 (1993).

[16] A.A. Sokolov and I.M. Ternov, Sov. Phys. Doklady **8** (1964) 1203.

[17] D.P. Barber *et al.*, Phys. Lett. B **343** (1995) 436.

[18] D.P. Barber *et al.*, Nucl. Instr. Meth. A **329** (1993) 79.

[19] A. Most, Proc. of the "12th International Symposium on High-Energy Spin Physics," edited by C.W. de Jager *et al.*, Amsterdam, The Netherlands, World Scientific (1997) 800.

[20] J. Stewart, Proc. of the Workshop "Polarized gas targets and polarized beams", edited by R.J. Holt and M.A. Miller, Urbana-Champaign, USA, AIP Conf. Proc. **421** (1997) 69.

[21] D. De Schepper *et al.*, Nucl. Instr. Meth. A **419** (1998) 16.

[22] F. Stock *et al.*, Nucl. Instr. Meth. A **343** (1994) 334.

[23] G.E. Thomas *et al.*, Nucl. Instr. Meth. A **257** (1987) 32.

[24] B. Braun, Proc. of the Workshop "Polarized gas targets and polarized beams", edited by R.J. Holt and M.A. Miller, Urbana-Champaign, USA, AIP Conf. Proc. **421** (1997) 156.

[25] HERMES, K. Ackerstaff *et al.*, Nucl. Instr. Meth. A **417** (1998) 230.

[26] J.L. Friar *et al.*, Phys. Rev. C **42** (1990) 2310.

[27] more details of the analysis can be found in H.A.M. Tallini, PhD thesis, Univ. Liverpool, (1998); M. Ruh, PhD thesis, Univ. Freiburg, (1999); B. Tipton, PhD thesis, MIT, Cambridge, (1999) and

[28] M.A. Funk, PhD thesis, Univ. Hamburg, ISSN 1435-8085 (1998).

[29] E-143, K. Abe *et al.*, Phys. Rev. D **58** (1998) 112003.

[30] E-155, P.L. Anthony *et al.*, SLAC-PUB-7983 (1999), hep-ex/9901006.

[31] I.V. Akushevich and N.M. Shumeiko, J. Phys. G: Nucl. Part. Phys. **20** (1994) 513.

[32] I.V. Akushevich *et al.*, Comp. Phys. Comm. **104** (1997) 201.

[33] Yu. G. Kolomensky, private communication.

[34] SMC, B. Adeva *et al.*, Phys. Lett. B **420** (1998) 180.

[35] J.M. Niczyporuk, E.E.W. Bruins, Phys. Rev. D **58** (1998) 091501.

[36] G. Ingelman, A. Edin, J. Rathsman, DESY Report 96-057 (1996).

[37] H.L. Lai *et al.*, Phys. Rev. D **55** (1997) 1280.

[38] L.W. Whitlow *et al.*, Phys. Lett. B **250** (1990) 193.

[39] C. Ciofi degli Atti *et al.*, Phys. Rev. C **48** (1993) R968.

[40] D. Diakonov *et al.*, Nucl. Phys. B **480** (1996) 341.

[41] R. Fries and A. Schäfer, hep-ph/9805509.

[42] M. Glück, E. Reya, A. Vogt, Z. Phys. C **67** (1995) 433.

[43] T. Sjöstrand, Comp. Phys. Comm. **82** (1994) 74.

[44] R.D. Field and R.P. Feynman, Nucl. Phys. B **136** (1978) 1.

[45] D. de Florian, O. Sampayo, R. Sassot, Phys. Rev. D **57** (1998) 5803.

[46] T. Gehrmann and W.J. Stirling, Phys. Rev. D **53** (1996) 6100.

[47] M. Glück *et al.*, Phys. Rev. D **53** (1996) 4775.

[48] R. Heimann, Nucl. Phys. B **64** (1973) 429.

[49] J. Ellis and M. Karliner, Phys. Lett. B **213** (1988) 73.

[50] J.D. Bjorken, Phys. Rev. **148** (1966) 1467; J.D. Bjorken, Phys. Rev. D **1** (1970) 1376.

[51] S.A. Larin, Phys. Lett. B **334** (1994) 192; A.L. Kataev, V.V. Starshenko, Mod. Phys. Lett. A**10**, (1995) 235.

[52] F.E. Close and R.G. Roberts, Phys. Lett. B **316** (1993) 165.

[53] E. Stein *et al.*, Phys. Lett. B **343** (1995) 369; Phys. Lett. B **353** (1995) 107.

[54] M. Meyer-Hermann *et al.*, Phys. Lett. B **383** (1996) 463; Erratum-ibid. **393** (1997) 487.

[55] X. Ji and W. Melnitchouk, Phys. Rev. D **56** (1997) 1.

[56] J. Balla, M.V. Polyakov, and C. Weiss; Nucl. Phys. B **510** (1998) 327.

[57] J. Ellis and R.L. Jaffe, Phys. Rev. D **9** (1974) 1444; Phys. Rev. D **10** (1974) 1669.

[58] J. Lichtenstadt and H.J. Lipkin, Phys. Lett. B **353** (1995) 119.

[59] M. Göckeler *et al.*, Phys. Lett. B **414**, (1997) 340.

[60] M. Göckeler *et al.*, Nucl. Phys. Proc. Suppl. B **53** (1997) 81.

TABLE III. Bin boundaries in the variable x.

Bin number	1	2	3	4	5	6	7	8	9
x-range	0.023-0.040	0.040-0.055	0.055-0.075	0.075-0.10	0.10-0.14	0.14-0.20	0.20-0.30	0.30-0.40	0.40-0.60

TABLE IV. The values of the inclusive proton asymmetry A_1 and semi-inclusive proton asymmetries for positively charged hadrons ($A_1^{h^+}$) and negatively charged hadrons ($A_1^{h^-}$). The values are quoted at the average measured values of x and Q^2 in each x-bin. The first error is statistical, the second one systematic.

$\langle x \rangle$	$\langle Q^2 \rangle$ $\left[(\mathrm{GeV}/c)^2 \right]$	$A_1 \pm$ stat. $\pm$ syst.
0.033	1.21	$0.078 \pm 0.006 \pm 0.006$
0.047	1.47	$0.104 \pm 0.007 \pm 0.008$
0.065	1.72	$0.117 \pm 0.008 \pm 0.009$
0.087	1.99	$0.163 \pm 0.009 \pm 0.012$
0.119	2.30	$0.194 \pm 0.009 \pm 0.015$
0.168	2.66	$0.240 \pm 0.011 \pm 0.019$
0.245	3.06	$0.307 \pm 0.014 \pm 0.025$
0.342	3.74	$0.415 \pm 0.023 \pm 0.034$
0.465	5.16	$0.552 \pm 0.032 \pm 0.048$

$\langle x \rangle$	$\langle Q^2 \rangle$ $\left[(\mathrm{GeV}/c)^2 \right]$	$A_1^{h^+} \pm$ stat. $\pm$ syst.
0.033	1.21	$0.087 \pm 0.016 \pm 0.006$
0.047	1.46	$0.111 \pm 0.017 \pm 0.008$
0.065	1.75	$0.136 \pm 0.017 \pm 0.010$
0.087	2.14	$0.180 \pm 0.019 \pm 0.013$
0.118	2.70	$0.247 \pm 0.020 \pm 0.018$
0.165	3.67	$0.245 \pm 0.024 \pm 0.019$
0.238	5.16	$0.411 \pm 0.033 \pm 0.031$
0.339	7.23	$0.403 \pm 0.066 \pm 0.033$
0.447	9.75	$0.619 \pm 0.132 \pm 0.053$

$\langle x \rangle$	$\langle Q^2 \rangle$ $\left[(\mathrm{GeV}/c)^2 \right]$	$A_1^{h^-} \pm$ stat. $\pm$ syst.
0.033	1.21	$0.049 \pm 0.020 \pm 0.004$
0.047	1.46	$0.094 \pm 0.021 \pm 0.007$
0.065	1.75	$0.066 \pm 0.022 \pm 0.005$
0.087	2.14	$0.060 \pm 0.025 \pm 0.006$
0.118	2.70	$0.181 \pm 0.027 \pm 0.014$
0.165	3.67	$0.194 \pm 0.034 \pm 0.016$
0.238	5.16	$0.213 \pm 0.048 \pm 0.019$
0.339	7.23	$0.572 \pm 0.100 \pm 0.043$
0.447	9.75	$0.111 \pm 0.203 \pm 0.031$

TABLE V. The values of the inclusive ^{3}He asymmetry A_1 and semi-inclusive ^{3}He asymmetries for positively charged hadrons $(A_1^{h^+})$ and negatively charged hadrons $(A_1^{h^-})$. The values are quoted at the average measured values of x and Q^2 in each x-bin. The first error is statistical, the second one systematic.

$\langle x \rangle$	$\langle Q^2 \rangle \quad \left[(\text{GeV}/c)^2 \right]$	$A_1 \pm$ stat.$\pm$ syst.
0.033	1.21	$-0.036 \pm 0.013 \pm 0.005$
0.047	1.47	$-0.009 \pm 0.014 \pm 0.003$
0.065	1.72	$-0.027 \pm 0.015 \pm 0.003$
0.087	1.99	$-0.025 \pm 0.018 \pm 0.003$
0.119	2.30	$-0.033 \pm 0.019 \pm 0.004$
0.168	2.66	$-0.037 \pm 0.023 \pm 0.005$
0.245	3.06	$-0.006 \pm 0.028 \pm 0.006$
0.342	3.74	$0.072 \pm 0.047 \pm 0.012$
0.465	5.16	$-0.021 \pm 0.066 \pm 0.019$

$\langle x \rangle$	$\langle Q^2 \rangle \quad \left[(\text{GeV}/c)^2 \right]$	$A_1^{h^+} \pm$ stat.$\pm$ syst.
0.033	1.21	$-0.051 \pm 0.032 \pm 0.007$
0.047	1.46	$-0.011 \pm 0.033 \pm 0.006$
0.065	1.75	$-0.030 \pm 0.034 \pm 0.006$
0.087	2.14	$-0.035 \pm 0.039 \pm 0.006$
0.118	2.70	$-0.024 \pm 0.041 \pm 0.006$
0.165	3.67	$0.006 \pm 0.048 \pm 0.006$
0.238	5.16	$-0.151 \pm 0.065 \pm 0.013$
0.339	7.23	$-0.088 \pm 0.133 \pm 0.013$
0.447	9.75	$-0.105 \pm 0.275 \pm 0.021$

$\langle x \rangle$	$\langle Q^2 \rangle \quad \left[(\text{GeV}/c)^2 \right]$	$A_1^{h^-} \pm$ stat.$\pm$ syst.
0.033	1.21	$-0.079 \pm 0.037 \pm 0.008$
0.047	1.46	$0.021 \pm 0.039 \pm 0.006$
0.065	1.75	$-0.021 \pm 0.042 \pm 0.006$
0.087	2.14	$0.027 \pm 0.049 \pm 0.006$
0.118	2.70	$0.009 \pm 0.052 \pm 0.006$
0.165	3.67	$-0.022 \pm 0.065 \pm 0.006$
0.238	5.16	$0.062 \pm 0.089 \pm 0.009$
0.339	7.23	$-0.220 \pm 0.191 \pm 0.019$
0.447	9.75	$0.293 \pm 0.616 \pm 0.028$

TABLE VI. The correlation coefficients ρ between the asymmetries. The proton and ^{3}He asymmetries are uncorrelated. The correlation coefficients between the inclusive and semi-inclusive asymmetries on each target are given by $\rho(A_1^{h^+}, A_1^{h^-}) = \langle n^+ n^- \rangle / \sqrt{\langle n^{+\,2} \rangle \langle n^{-\,2} \rangle}$ and $\rho(A_1, A_1^{h^{+(-)}}) = \langle n^{+(-)} \rangle / \sqrt{\langle n^{+(-)\,2} \rangle}$, where $n^{+(-)}$ is the number of positively (negatively) charged hadrons per scattered positron.

$\langle x \rangle$	$\rho(A_{1\text{p}}, A_{1\text{p}}^{h^+})$	$\rho(A_{1\text{p}}, A_{1\text{p}}^{h^-})$	$\rho(A_{1\text{p}}^{h^+}, A_{1\text{p}}^{h^-})$	$\rho(A_{1\text{He}}, A_{1\text{He}}^{h^+})$	$\rho(A_{1\text{He}}, A_{1\text{He}}^{h^-})$	$\rho(A_{1\text{He}}^{h^+}, A_{1\text{He}}^{h^-})$
0.033	0.452	0.394	0.130	0.446	0.395	0.128
0.047	0.490	0.414	0.140	0.491	0.417	0.137
0.065	0.517	0.406	0.134	0.507	0.411	0.131
0.087	0.509	0.379	0.120	0.497	0.386	0.117
0.119	0.464	0.328	0.108	0.452	0.336	0.105
0.168	0.375	0.253	0.098	0.365	0.260	0.096
0.245	0.267	0.171	0.084	0.260	0.178	0.083
0.342	0.188	0.115	0.066	0.183	0.120	0.066
0.465	0.130	0.076	0.050	0.127	0.080	0.051

TABLE VII. The **flavor decomposition** $(\Delta u + \Delta\bar{u})/(u + \bar{u})$, $(\Delta d + \Delta\bar{d})/(d + \bar{d})$, and $\Delta q_{\rm s}/q_{\rm s}$ of the quark polarization as a function of x derived from the HERMES inclusive and semi-inclusive asymmetries on the ^{3}He and proton targets. The first error is statistical and the second one systematic. The values were obtained with the assumption that the sea quark polarization is flavor symmetric.

$\langle x \rangle$	$\frac{\Delta u + \Delta\bar{u}}{u + \bar{u}} \pm$ stat.$\pm$ syst.	$\frac{\Delta d + \Delta\bar{d}}{d + \bar{d}} \pm$ stat.$\pm$ syst.	$\Delta q_{\rm s}/q_{\rm s} \pm$ stat.$\pm$ syst.
0.033	$0.103 \pm 0.013 \pm 0.010$	$-0.126 \pm 0.052 \pm 0.021$	$0.012 \pm 0.095 \pm 0.042$
0.047	$0.108 \pm 0.014 \pm 0.007$	$-0.063 \pm 0.057 \pm 0.016$	$0.109 \pm 0.103 \pm 0.039$
0.065	$0.143 \pm 0.014 \pm 0.011$	$-0.127 \pm 0.063 \pm 0.017$	$-0.055 \pm 0.121 \pm 0.068$
0.087	$0.192 \pm 0.016 \pm 0.013$	$-0.143 \pm 0.077 \pm 0.016$	$-0.215 \pm 0.169 \pm 0.117$
0.119	$0.215 \pm 0.017 \pm 0.014$	$-0.209 \pm 0.090 \pm 0.026$	$0.148 \pm 0.236 \pm 0.119$
0.168	$0.260 \pm 0.021 \pm 0.019$	$-0.239 \pm 0.123 \pm 0.050$	$0.200 \pm 0.441 \pm 0.137$
0.245	$0.348 \pm 0.027 \pm 0.022$	$-0.235 \pm 0.191 \pm 0.078$	$-1.108 \pm 1.077 \pm 0.691$
0.342	$0.374 \pm 0.043 \pm 0.025$	$0.478 \pm 0.388 \pm 0.085$	
0.465	$0.656 \pm 0.063 \pm 0.039$	$-0.989 \pm 0.787 \pm 0.129$	

TABLE VIII. Statistical correlation coefficients ρ between the quark polarizations $(\Delta u + \Delta\bar{u})/(u + \bar{u})$, $(\Delta d + \Delta\bar{d})/(d + \bar{d})$, and $\Delta q_{\rm s}/q_{\rm s}$ in each x-bin. Also shown is the $\chi^2_{\min}$ of the fit. The number of degrees of freedom of the fit is six for the bins 1 to 7 and seven for the bins 8 and 9.

$\langle x \rangle$	$\rho\left(\frac{\Delta u + \Delta\bar{u}}{u + \bar{u}}, \frac{\Delta d + \Delta\bar{d}}{d + \bar{d}}\right)$	$\rho\left(\frac{\Delta u + \Delta\bar{u}}{u + \bar{u}}, \frac{\Delta q_{\rm s}}{q_{\rm s}}\right)$	$\rho\left(\frac{\Delta d + \Delta\bar{d}}{d + \bar{d}}, \frac{\Delta q_{\rm s}}{q_{\rm s}}\right)$	$\chi^2_{\min}$
0.033	-0.76	-0.12	-0.38	5.4
0.047	-0.76	-0.04	-0.40	1.0
0.065	-0.76	-0.02	-0.42	0.5
0.087	-0.75	-0.02	-0.44	11.2
0.119	-0.73	-0.05	-0.46	7.9
0.168	-0.69	-0.11	-0.47	5.1
0.245	-0.57	-0.31	-0.45	13.3
0.342	-0.84			11.6
0.465	-0.85			5.4

TABLE IX. The **valence decomposition** $\Delta u_{\mathrm{v}}/u_{\mathrm{v}}$, $\Delta d_{\mathrm{v}}/d_{\mathrm{v}}$ and $\Delta q_{\mathrm{s}}/q_{\mathrm{s}}$ of the quark polarization as a function of x, derived from the HERMES inclusive and semi-inclusive asymmetries on the ^{3}He and proton targets. The first error is statistical and the second one systematic. The values were obtained with the assumption that the sea quark polarization is flavor symmetric.

$\langle x \rangle$	$\Delta u_{\mathrm{v}}/u_{\mathrm{v}} \pm$ stat.$\pm$ syst.	$\Delta d_{\mathrm{v}}/d_{\mathrm{v}} \pm$ stat.$\pm$ syst.	$\Delta q_{\mathrm{s}}/q_{\mathrm{s}} \pm$ stat.$\pm$ syst.
0.033	$0.215 \pm 0.122 \pm 0.060$	$-0.421 \pm 0.306 \pm 0.113$	$0.012 \pm 0.095 \pm 0.039$
0.047	$0.108 \pm 0.094 \pm 0.039$	$-0.354 \pm 0.274 \pm 0.111$	$0.109 \pm 0.103 \pm 0.040$
0.065	$0.269 \pm 0.081 \pm 0.055$	$-0.225 \pm 0.266 \pm 0.106$	$-0.055 \pm 0.121 \pm 0.068$
0.087	$0.374 \pm 0.080 \pm 0.062$	$-0.064 \pm 0.297 \pm 0.151$	$-0.215 \pm 0.169 \pm 0.119$
0.119	$0.234 \pm 0.073 \pm 0.050$	$-0.519 \pm 0.320 \pm 0.098$	$0.148 \pm 0.236 \pm 0.122$
0.168	$0.270 \pm 0.079 \pm 0.041$	$-0.520 \pm 0.418 \pm 0.114$	$0.200 \pm 0.441 \pm 0.148$
0.245	$0.456 \pm 0.093 \pm 0.071$	$0.136 \pm 0.630 \pm 0.437$	$-1.108 \pm 1.077 \pm 0.717$
0.342	$0.385 \pm 0.045 \pm 0.026$	$0.602 \pm 0.489 \pm 0.264$	
0.465	$0.663 \pm 0.064 \pm 0.040$	$-1.127 \pm 0.897 \pm 0.220$	

TABLE X. Statistical correlation coefficients ρ between the quark polarizations $\Delta u_{\mathrm{v}}/u_{\mathrm{v}}$, $\Delta d_{\mathrm{v}}/d_{\mathrm{v}}$ and $\Delta q_{\mathrm{s}}/q_{\mathrm{s}}$ in each x-bin. Also shown is the χ^2_{min} of the fit. The number of degrees of freedom of the fit is six for the bins 1 to 7 and seven for the bins 8 and 9.

$\langle x \rangle$	$\rho\left(\Delta u_{\mathrm{v}}/u_{\mathrm{v}}, \Delta d_{\mathrm{v}}/d_{\mathrm{v}}\right)$	$\rho\left(\Delta u_{\mathrm{v}}/u_{\mathrm{v}}, \Delta q_{\mathrm{s}}/q_{\mathrm{s}}\right)$	$\rho\left(\Delta d_{\mathrm{v}}/d_{\mathrm{v}}, \Delta q_{\mathrm{s}}/q_{\mathrm{s}}\right)$	χ^2_{min}
0.033	0.74	-0.98	-0.87	5.4
0.047	0.71	-0.96	-0.86	1.0
0.065	0.70	-0.96	-0.86	0.5
0.087	0.71	-0.96	-0.87	11.2
0.119	0.72	-0.95	-0.88	7.9
0.168	0.75	-0.95	-0.90	5.1
0.245	0.79	-0.96	-0.92	13.3
0.342	-0.84			11.6
0.465	-0.85			5.4